Environ Fluid Mech (2014) 14:1229–1249
DOI 10.1007/s10652-013-9294-3

ORIGINAL ARTICLE

Spatial structure of internal Poincaré waves in Lake Michigan

Sultan Ahmed · Cary D. Troy · Nathan Hawley

Received: 8 February 2013 / Accepted: 3 June 2013 / Published online: 18 June 2013

Abstract In this paper we examine the characteristics of near-inertial internal Poincaré waves in Lake Michigan (USA) as discerned from field experiments and hydrodynamic simulations. The focus is on the determination of the lateral and vertical structure of the waves. Observations of near-inertial internal wave properties are presented from two field experiments in southern Lake Michigan conducted during the years 2009 and 2010 at Michigan City (IN, USA) and Muskegon (MI, USA), respectively. Spectra of thermocline displacements and baroclinic velocities show that kinetic and potential baroclinic energy is dominated by near-inertial internal Poincaré waves. Vertical structure discerned from empirical orthogonal function analysis shows that this energy is predominantly vertical mode 1. Idealized hydrodynamic simulations using stratifications from early summer (June), mid-summer (July) and fall (September) identify the basin-scale internal Poincaré wave structure as a combination of single- and two-basin cells, similar to those identified in Lake Erie by Schwab, with near-surface velocities largest in the center of the northern and southern basins. Near-inertial bottom kinetic energy is seen to have roughly constant magnitude over large swathes across the basin, with higher magnitude in the shallower areas like the Mid-lake Plateau, as compared with the deep northern and southern basins. The near-bottom near-inertial kinetic energy when mapped appears similar to the bottom topography map. The wave-induced vertical shear across thermocline is concentrated along the longitudinal axis of the lake basin, and both near-bottom velocities and thermocline shear are reasonably explained by a simple conceptual model of the expected transverse variability.

Keywords Internal waves · Seiches · Poincaré waves · Lakes · Near-inertial waves

S. Ahmed · C. D. Troy (✉)
School of Civil Engineering, Purdue University, West Lafayette, IN, USA
e-mail: troy@purdue.edu

N. Hawley
NOAA Great Lakes Environmental Research Lab, Ann Arbor, MI, USA

1 Introduction

A long internal wave response is initiated in a lake basin when the tilted metalimnion overshoots the equilibrium position, after the wind duration exceeds one quarter of the basin scale internal wave period [1]. It has been established that the energy path transferring mechanical energy from the wind down to the smallest scales of motion in a stratified lake begins with the baroclinic basin-scale motions [2]. Basin-scale internal waves transfer the energy introduced by winds to the bottom boundary layer [3], cause resuspension of sediments [4,5], enhance mass transfer at the sediment–water interface [6], and enhance near-bottom mixing [7,8]. The locations where these effects are important are set largely by the spatial structure of the dominant internal seiche response, which in turn is very lake-specific.

The earth's rotation has an important effect on internal seiches when the internal Burger number becomes small ($S_i = c_i/fL$ where c_i is the long internal wave speed, f is the Coriolis parameter, and L is the basin scale [9]). When this is the case, the baroclinic basin-scale response to external forcing is primarily in the form of internal sub-inertial Kelvin waves and super-inertial Poincaré waves. In flat-bottomed, circular or elliptical basins, numerous radial, vertical, and azimuthal modes are possible.

Csanady [10] and Antenucci and Imberger [9] derived the dispersion relations for linear long waves in a rotating circular basin. In an idealized circular, flat-bottomed lake, the shape of lowest radial mode excited by a uniform wind has positive isothermal displacement on one side and negative isothermal displacement on the other side, with anti-cyclonic propagation around the lake. Velocities are in phase everywhere across the basin, with largest magnitude in the lake center, and currents flowing in the opposite direction on either side of the thermocline for the lowest vertical mode.

Bathymetry plays an important role in determining the spatial structure of excited non-rotational internal seiches [11] and this is also true for (rotational) internal Poincaré waves. For lakes with multiple basins, unique Poincaré cells tend to form in the separate basins [12], which is also found here for Lake Michigan. Schwab's [13] semi-analytical calculations of internal Poincaré wave structure in a flat-bottomed Lake Ontario revealed the fundamental response to include a whole-basin mode and multiple-basin modes.

In very large lakes with low Burger number such as the Laurentian Great Lakes, all internal Poincaré modes converge to the inertial frequency/period (18.0 h for southern Lake Michigan), and near-inertial currents are observed to dominate the lake interior [14–18]. For these large lakes, individual Poincaré modes for these lakes are nearly impossible to separate spectrally because of the nearly-identical periods for the dominant modes and the non-stationarity associated with changing wind and stratification, which essentially makes the dominant wave structure and periods temporally-evolving targets.

Recent work by Choi et al. [17] showed that observed currents in Lake Michigan's interior are thoroughly dominated by near-inertial internal Poincaré waves from May through December, efficiently absorbing wind energy with near-surface velocities approaching 50cm/s during the most energetic episodes. The regularity of these periodic currents was shown to be almost tide-like, with slow evolution of wave phase with wind events. Estimated Richardson numbers suggested that these waves were sufficiently strong to drive thermocline mixing, which Bouffard et al. [19] recently established directly with microstructure measurements for Lake Erie. This suggests that the magnitude of internal Poincaré wave-induced thermocline mixing is quite significant in the lake interior.

In this paper, the spatial structure of internal Poincaré waves in Lake Michigan is examined using results from field experiments and hydrodynamic simulations. Results are phrased in terms of thermocline displacements, surface and bottom velocities, and thermocline shear,

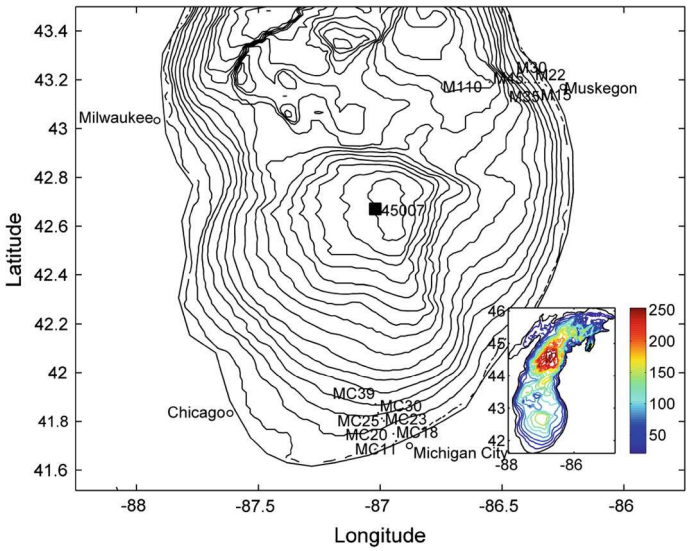

Fig. 1 Field experiment locations in southern Lake Michigan during summer 2009 near Michigan City (MC#), Indiana (USA) and during summer 2010 near Muskegon (M#), Michigan (USA). Contours are shown at 10 m intervals. *Inset* shows the bathymetry of Lake Michigan, with the *color bar* depicting depth in meters

in order to better understand the linkages between the basic Poincaré spatial structure and the expected effects on lateral dispersion, benthic exchange and resuspension, and vertical mixing.

2 Observations

Lake Michigan (Fig. 1) is the second largest Great Lake in North America. It has a maximum length of 494 km, a maximum width of 190 km, an average depth of 85 m and a maximum depth of 281 m. It has two main basins; the Chippewa Basin in the north is separated from the South Chippewa Basin by the mid-lake plateau, which is located at about 43° N (roughly from Milwaukee to Muskegon). Bathymetry in the Southern Chippewa Basin is gently sloping along the Illinois and Indiana coastline with 40 m depth reached approximately 20 km offshore, while it is steep on the eastern Michigan side with 110 m depth reached approximately 20 km offshore (Fig. 1).

Results from two field experiments are presented herein; one experiment was carried out near Michigan City, IN (USA; hereafter "MC2009") in summer of 2009, and the second experiment was carried out near Muskegon, MI (USA; hereafter "MUSK2010") in summer of 2010 (Fig. 1; Table 1). Both of these experiments involved temperature measurements along cross-shelf transects which extended approximately 20 km offshore. The Michigan City location has a mild slope (40 m: 20 km, 0.002) whereas the Muskegon location has a more typical shelf slope (110 m: 20 km, 0.006).

The MC2009 experiment included seven thermistor chains at depths 11, 18, 20, 23, 25, 30 and 40 m, with an ADCP near the 30 m station (offshore distance = 15 km). The MUSK2010 transect had six thermistor chains at 17, 22, 30, 35, 45 and 107m depths. ADCP's deployed along the Muskegon transect were fouled and did not return any usable data. More details about the 2009 summer field experiment can be found in Troy et al. [20].

Table 1 Locations and details of various moorings and instruments deployed during 2009 and 2010 field experiments in southern Lake Michigan near Michigan City, IN (USA) and Muskegon, Michigan (USA)

Mooring	Depth (m)	Offshore Distance (km)	Thermistors (#)	ADCP	Latitude/longitude
MC11	11	1.2	5	–	41.7197N, 86.9341W
MC18	18	4.6	6	–	41.7491N, 86.9456W
MC20	20	8.9	8	–	41.7823N, 86.9744W
MC23	23	11.3	8	–	41.8023N, 86.9853W
MC25	25	12.6	9	–	41.8120N, 86.9935W
MC30	30	15.3	10	Yes↑	41.8346N, 87.0085W
MC39	39	19.6	14	–	41.8707N, 87.0198W
M15	17	2.7	7	Yes↑	43.1882N, 86.3481W
M22	22.1	3.9	7	–	43.1895N, 86.3647W
M30	30.5	5.8	10	–	43.1909N, 86.3912W
M35	35.1	6.8	11	–	43.1895N, 86.4054W
M45	46.4	9.2	19	–	43.1880N, 86.4390W
M110	107	19.6	22	–	43.1913N, 86.5521W

↑ Upward looking ADCP

MUSK2010 lasted from 06 April 2010 till 22 September 2010, which correspond to the Julian days (hereafter "DOY") 96–265 of the year 2010. Temperature sensors at M110, M45 and M15 were deployed on 06 April while the M22, M30 and M35 were deployed on 22 June 2010 (Fig. 2). RBR-TDRs, SeaBird 39s, and Onset U22 Pro v2s were used in the summer 2010 experiment. SeaBirds and Onset U22 Pro v2s logged data at 10 min interval and the RBRs recorded the data at 10 s interval. The response time of the instruments is 5 min for

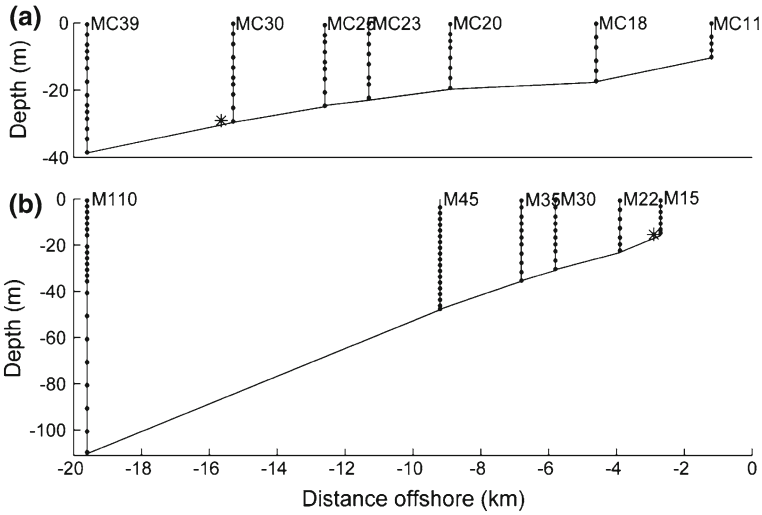

Fig. 2 Vertical distribution of thermistors and ADCPs during **a** MC2009 and **b** MUSK2010 experiments. ADCP locations are shown by *asterisk*. Meaningful data was not obtained from MUSK2010 ADCPs at 45 and 110 m depths due to fouling/tipping of the ADCPs

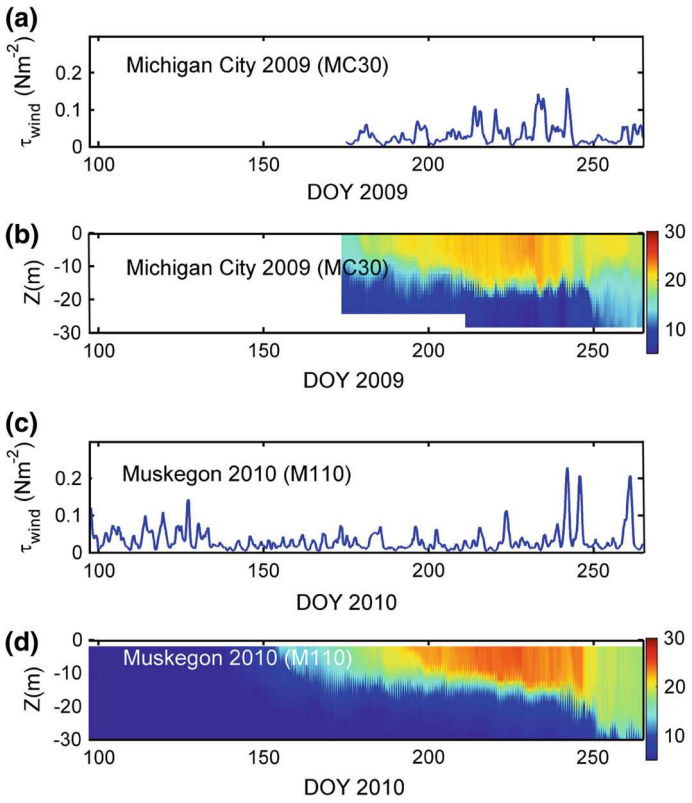

Fig. 3 **a** Wind stress from Michigan City weather station during 2009, **b** thermal stratification from MC30 location during the 2009 experiment, **c** wind stress from Muskegon weather station during 2010 and **d** thermal stratification from M110 location during the 2010 experiment. The *color bars* show water temperature. For clarity, same depths are shown in *panels* **b** and **d**

U22s and 0.1 s for RBRs. Meaningful records on M35 were made only until August 4, 2010 when it became unmoored.

Meteorological data was obtained from the NOAA Michigan City and Muskegon stations (MCYI3, 41.729°N, 86.913°W; MKGM4, 43.216°N, 86.338°W). Additional weather data was obtained from NOAA buoy 45007 (42.674°N, 87.026°W) which is located in the center of the southern basin (Fig. 1). This buoy also recorded surface water temperature, wave height, wave period, and wave direction each hour. All wind speeds were adjusted to 10m height using a wind speed–dependent drag coefficient, which was also used to estimate wind stress [21].

Figure 3 shows the wind stress at MC and MUSK, along with the temperatures at the stations, MC30 and M110. Both stations show the general seasonal trends seen in winds and stratification (e.g. [22]). Temperature data at M110 shows nearly well mixed conditions during April, with the onset of persistent stratification in early June, the strengthening and slow deepening of the thermocline through early September, and the eventual weakening of the thermocline during September due to weaker solar radiation and stronger winds. During the strongly-stratified months of July and August, the thermocline lies between 15 and 20 m depth for both locations. Near-inertial oscillations in the thermocline can be seen at both locations.

Table 2 Episodes of intense near-inertial activity which were investigated using EOF from MC30 mooring data during 2009 are shown. Also shown are the variances explained by the EOF modes and the dominant period of those modes

Episode (DOY)	EOF mode 1, 2 variances (%)	EOF mode 1, 2 dominant periods (h)
195–203	85, 5	17.8, 9.0
205–214	89, 5	17.8, 8.9
221–232	68, 12	17.8, (17.8,8.7)
237–247	78, 8	17.8, (17.8,8.7)
252–265	87, 5	17.8, (15.4,9.0)

2.1 Vertical structure

The vertical structure of the internal wave-induced currents was examined using the 2009 ADCP data from Michigan City, 30 m depth (no velocity data was available for 2010). Empirical orthogonal function (EOF) analysis was carried out on the ADCP-derived velocity profiles in order to determine the dominant baroclinic structure (e.g. [23]). EOF analysis has the advantage of making no a priori assumptions regarding the vertical structure and causes of the observed velocity profiles, and simply provides a least squares determination of the dominant orthogonal functions forming the basis of the observed velocity profiles. The analysis was carried out on the complex velocity fields $u(z,t)+iv(z,t)$ in order to elucidate the two-dimensional structure of the dominant modes that was seen in visualizations of the raw data, following Kundu and Allen [24]. This is an important distinction in our analysis; for rotating velocity profiles with two-dimensional structure as we find below, EOF analysis carried out separately on the east and north velocity components will spuriously find mode 2 energy that is actually indicative of two-dimensional, spiraling structure (one can detect this in cases when the analysis is carried out separately on each velocity component by noting that the amplitudes of EOF modes 1 and 2 are generally phase-locked).

Because baroclinic structure can exist in low-frequency features such as coastal jets [20] and density intrusions, the filtered high-pass (super-inertial) velocities were used in order to isolate the vertical structure of internal wave-induced motions. Since the vertical structure associated with baroclinic modes is set by the thermal stratification, which varied over the course of the experiment, the record was broken into distinct episodes of energetic baroclinic activity over which the thermal stratification and vertical velocity structure were observed to be vertically stationary in the water column (Table 2). This use of shorter sub-records prevents the aliasing of non-stationarity into spurious EOF modes/energy. However, if one blindly uses the entire record without any regard for non-stationarity, the conclusions presented below do not change: the EOF-derived first mode, which resembles vertical mode 1, still thoroughly dominates the record, accounting for 75 % of the variance of the super-inertial velocities, with the same general vertical structure as described below. The use of shorter records simply increases the percentage of energy attributed to the lowest mode, because the lowest mode shape is more finely tuned for each particular period.

Near-inertial, baroclinic mode 1 structure was found to dominate the vertical current structure for the entirety of the 2009 Michigan City record (Table 2; Fig. 4). The spectrally-determined dominant period of mode 1 waves is approximately 17.8 h, in keeping with the near-inertial periods for lowest mode internal Poincaré waves typically found in the basin [17]. Some mode 1 energy is seen at a less-distinct period of 16.8 h. The variances attributed to this mode approach 90 % for the most energetic episodes; episodes with lower variances have lower overall energy, with a more equal distribution of energy among many lower EOF modes. Additionally, for these low-energy episodes there is some phase-locked near-inertial

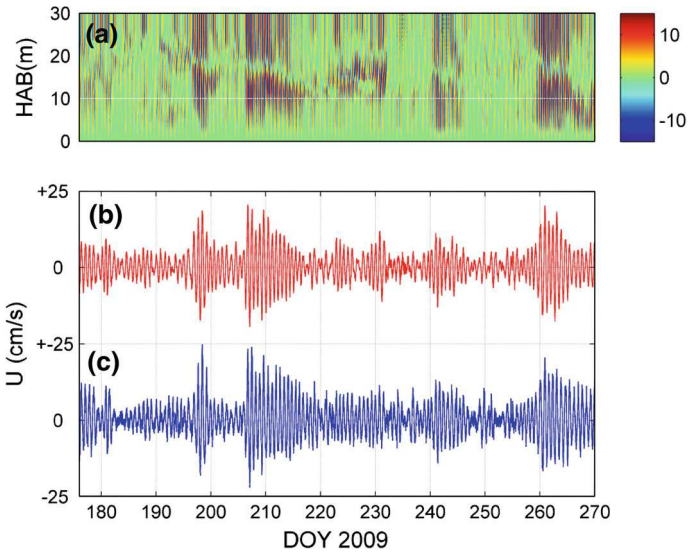

Fig. 4 **a** Super-inertial eastward velocities from MC30 for whole water column (cm/s), **b** raw eastward velocity data at 10 m elevation and **c** EOF vertical mode 1 reconstructed eastward velocity at 10 m elevation. Mode 1 accounts for more than 70 % of the observed variability, even when the entire record is used for the analysis and non-stationarity is ignored

energy in EOF mode 2, suggesting some aliasing of true mode 1 energy into the EOF-derived mode 2 (mode 2 is described later in this section).

Shown in Figs. 5 and 6 are the results of the EOF analysis for a particularly strong period of internal wave activity, DOY 205–214 (2009). The dominant EOF mode, shown in Fig. 6, captures 89 % of the variance for this period, and has a clearly discernible period of 17.8 h. The real and imaginary amplitudes for this mode are 90° out of phase and phase-locked, which creates the clockwise rotation of the velocity field over the near-inertial period, as observed in the raw data.

The shape of EOF mode 1 reveals the true two-dimensional baroclinic mode 1 vertical structure of the dominant Poincaré waves as can be seen by eye in the raw data (Fig. 6): oppositely directed velocities above and below the thermocline, spiraling velocities through the thermocline transitioning from the surface mixed layer to the hypolimnion, with the whole pattern rotating clockwise at near-inertial period. Additionally, the hypolimnetic velocities show a boundary layer structure as expected. With the exception of the spiral within the thermocline and the bottom boundary layer, the found mode 1 was seen to match the inviscid normal modes solution for all episodes examined.

Visualizations of the raw velocity fields confirm the spiraling (veering) seen in the found EOF mode 1; this spiral is phase-locked with the normal baroclinic structure expected for a vertical mode 1 wave (Fig. 6). The spiraling velocities are most likely a frictional effect, effectively an unsteady Ekman spiral within the thermocline and the bottom boundary layer. This feature—spiraling velocities as one descends through the thermocline—is a persistent feature of low-mode internal waves in Lake Michigan, even for deep waters where the thermocline is far from the influence of the lake bottom (Troy and Hawley, unpublished data). Ongoing work seeks to quantitatively relate this spiral to turbulent mixing rates within the thermocline and bottom boundary layer.

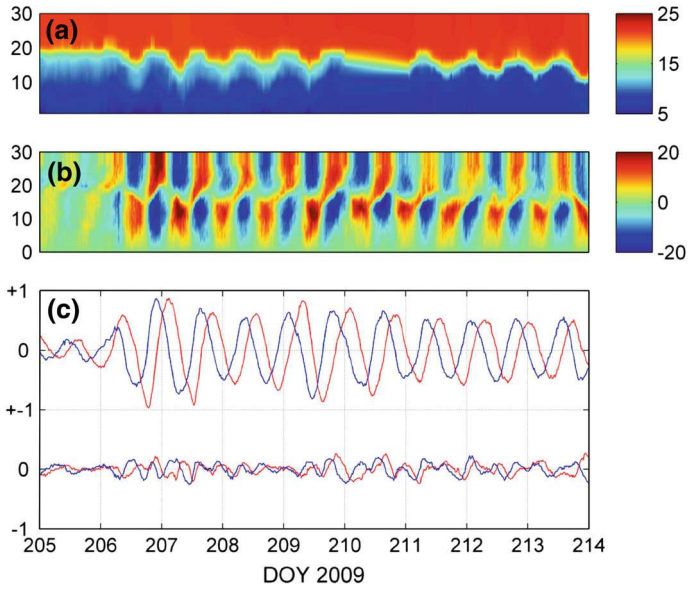

Fig. 5 **a** Water temperature (*y*-axis: elevation in m, color bar units: °C), linearly interpolated during DOY 210–211, **b** super-inertial north velocity (*y*-axis: elevation in m, *color bar* units: cm/s), and **c** found EOF mode 1 and 2 amplitude time series (*y*-axis: dimensionless) for MC30 during a period of intense near-inertial wave activity. EOF modes 1 and 2 (*top* and *bottom* time series of *panel* **c**, respectively) contain 91 and 4 % of the total variance for this episode, respectively; EOF mode 1 has a dominant period of approximately 17.7 h, whereas the EOF mode 2 period is approximately 8.9 h. The vertical structure of EOF mode 1 is shown in Fig. 7

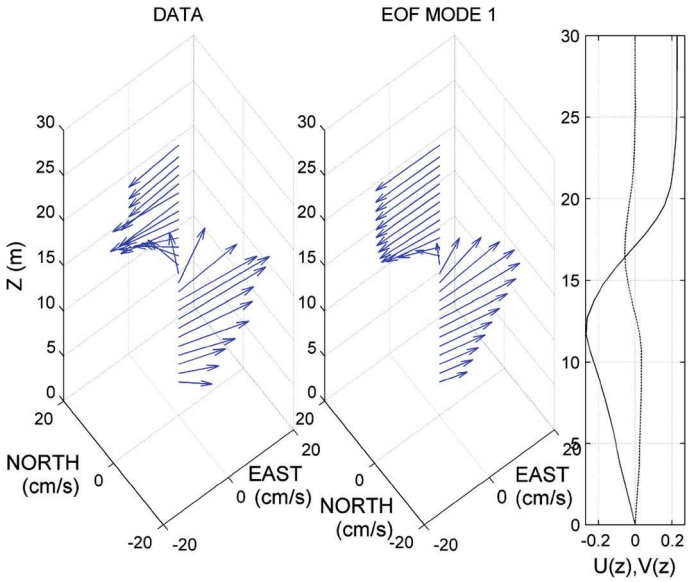

Fig. 6 Velocity profile and scaled EOF mode 1 for DOY 209.65. EOF mode 1 has baroclinic mode 1 structure, with oppositely-directed velocities above and below the thermocline, a bottom boundary layer structure, and spiraling velocities through the thermocline and into the bottom boundary layer. The whole profile rotates clockwise at a period of approximately 17.8 h

The EOF analysis performed on the complex velocity fields finds 5–10 % of the variance in a second mode for various episodes, which sometimes has weak near-inertial periodicity and sometimes has an approximate period of 8.9 h (i.e. first harmonic of the primary near-inertial wave). However, no energy is seen in the raw velocity spectra at this harmonic period, and so it is likely that the EOF mode 2 is simply an artifact of the EOF analysis, explaining additional variance not captured by the first mode. Additionally, the vertical structure of EOF-found mode 2—while consistent—is not readily explained by any physical process, with velocities 90° out of phase above and below the thermocline, and a broad spiraling region near the thermocline. Therefore, it is concluded that the EOF analysis does not show any plausible baroclinic mode 2 energy.

2.2 Cross-shelf variability

In order to examine cross-shelf variability in the Poincaré wave, integrated potential energy was used as a local metric of near-inertial internal wave activity at different moorings. Integrated potential energy (IPE; $\mathrm{J/m^2}$) is defined as

$$IPE \equiv \int_0^H \rho(z) g z dz \tag{1}$$

where ρ(z) is the vertical profile of density, derived from the temperature moorings; g is gravity; and z is the vertical coordinate positive upwards. As applied to temperature moorings that do not resolve free surface deflections, H is the mean depth of the water at the mooring during the experiment. As calculated, *IPE* changes at a given location are then due entirely to temperature changes in the water column, caused either by heating/cooling or from baroclinic (internal wave) activity. It is primarily influenced by isotherm deflections [25], but has the advantage of incorporating all thermal measurements at a mooring. Additionally, it is a time-continuous calculation that does not require the presence of a given isotherm.

For a two-layer fluid with hypolimnion and epilimnion depths of h' and h respectively, the potential energy change associated with an interfacial deflection η is [9]:

$$IPE(t) = \frac{\Delta\rho g}{2}\left(2h'\eta + \eta^2\right) \tag{2}$$

where $\Delta\rho = \rho' - \rho$ is the density difference between the bottom and top layers, respectively, and $\eta(t)$ is the local thermocline deflection. For purely harmonic (e.g. near-inertial) thermocline displacements of η_0, (2) is dominated by the first term, and the effective thermocline displacement $\eta(t)$ from internal waves is

$$\eta(t) = IPE/\Delta\rho g h' \tag{3}$$

For this conversion, average mooring stratification values were used over the experiments, which were found to be $\Delta\rho = 1.5\,\mathrm{kg/m^3}$ with $\mathrm{H}-\mathrm{h}' = 15\,\mathrm{m}$ for Michigan City, and $\Delta\rho = 2.1\,\mathrm{kg/m^3}$ with $\mathrm{H}-\mathrm{h}' = 16\,\mathrm{m}$ for Muskegon (H is the total local water depth).

The effective thermocline displacement η(t) (3) is used in lieu of the actual estimated thermocline displacement or *IPE* directly because the IPE-derived thermocline displacement is a whole water column metric that utilizes all thermistors on an array, and is therefore less dependent on individual pairs of sensors and their spacing. The effective displacement was a cleaner signal than the estimated raw thermocline displacement for most of the experiment. Additionally, while *IPE* has been used previously to quantify internal wave energy in

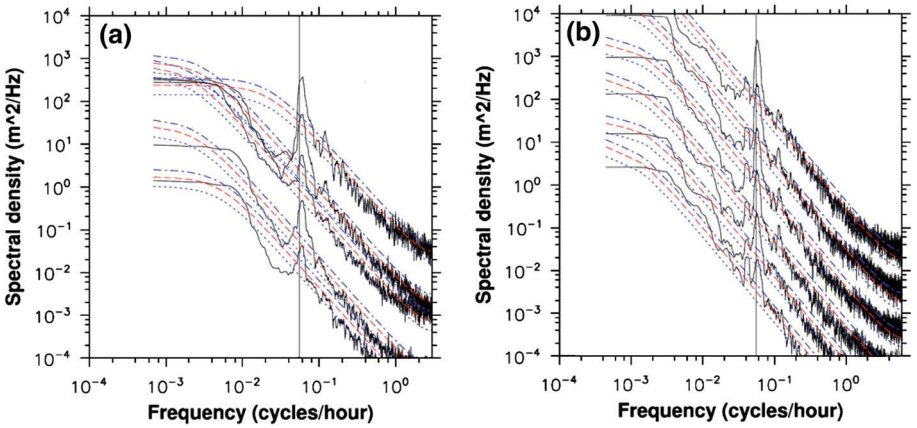

Fig. 7 Thermocline displacement (η) spectra from cross-shelf transect moorings at **a** Muskegon, 2010 (22, 30, 35, 45, 107 m depths) and **b** Michigan City, 2009 (18, 20, 23, 25, 30, 39 m depths). A well-defined near-inertial peak dominates the displacements, with the inertial frequency shown by the *vertical line*. Spectra are each offset by 1 decade, with the highest spectral density being that of the farthest mooring from the shore. The *dotted lines* show *red* noise curve and the confidence bounds

lakes (e.g. [9,25]), it is not useful here to discern cross-shelf structure because the hypolimnetic depth dependence in (2) means that measurements in deeper water will show elevated near-inertial IPE simply because of the increased depth, even after detrending or filtering.

The spectra associated with effective thermocline displacements during MC2009 and MUSK2010 are shown in Fig. 7. The dominant variability in all offshore thermocline displacement signals is at near-inertial frequency, with an average spectral near-inertial peak period of 17.28 h (slightly less than the local inertial period of 17.97 h). Additionally, both spectra show energy at a near-inertial first harmonic ($\sim$9.5 h), which is a consequence of the harmonic term in (2). The data from Michigan City also has some energy at the diurnal period, which is likely related to the shallow nature of the lake shelf at this site and the greater relative importance of diurnal heating and cooling.

Shown in Fig. 8 is the average thermocline displacement amplitude for the records during MC2009 and MUSK2010, showing the cross-shelf structure of thermocline displacement over the 20 km long transect. Thermocline displacements associated with these waves are small, with amplitudes rarely exceeding 3 m (not shown); this is in keeping with the near-inertial character of the waves, which mostly manifest themselves in currents (kinetic energy) and not isotherm deflections (potential energy) [9].

Very little isotherm deflection variability exists in the cross-shelf direction. The lowest-mode Poincaré wave in a flat-bottom basin is expected to have roughly maximum thermocline displacement near the shore, and the observations here suggest that this distribution may hold additionally for real bathymetry. It must be noted that the amplitudes shown here are not necessarily the lowest-mode wave amplitudes, and could represent the combination of several of the lowest near-inertial modes, averaged over the entire experiment.

3 Poincaré mode identification through idealized simulations

A key question related to internal Poincaré waves in Lake Michigan is the spatial structure of the dominant modes, which will govern the distribution of kinetic energy associated with the

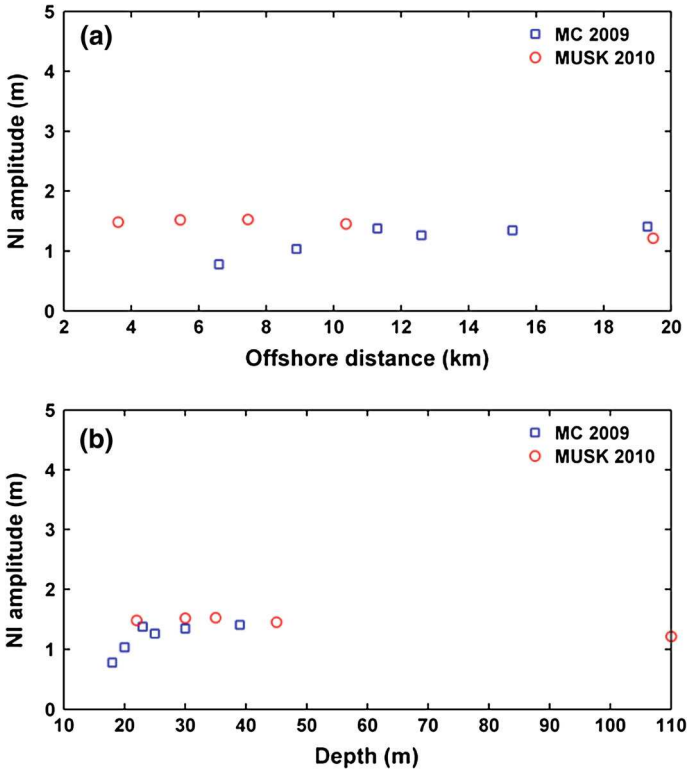

Fig. 8 Near-inertial thermocline vertical deflection amplitude magnitudes for Michigan City (2009) and Muskegon (2010). Shown are near-amplitude versus **a** offshore distance and **b** water depth, scaled to the approximate maximum isotherm deflections seen in the experiments (±5 m). Very little cross-shelf variation is seen, with no evidence of elevated wave amplitudes near the thermocline-shelf intersection

waves, and their subsequent influence on lateral dispersion, benthic exchange, and vertical mixing. Mortimer [15,16] examined the cross-shelf isotherms along the west-east Milwaukee (WI)–Muskegon (MI) transect and found a combination of first and fifth Poincaré cross-basin modes, with the first mode being equivalent to a half sine wave fit along the transect.

The experiments discussed earlier were spatially localized, and not suitable for the delineation of the basin-scale modal structure. In order to elucidate the large-scale spatial structure associated with near-inertial internal Poincaré waves in Lake Michigan, idealized three-dimensional numerical simulations were performed using the Stanford unstructured non-hydrostatic terrain-following adaptive navier-stokes simulator (SUNTANS; [26]). Modifications to the code as adapted here for Lake Michigan are described in detail in Ahmed [27].

The model was validated with the idealized upwelling/Kelvin wave test case of Beletsky et al. [28], for both a 100 km diameter circular lake and Lake Michigan; the results show very good agreement with the published upwelling and internal Kelvin wave propagation features (Ahmed, in preparation).

3.1 Model setup and analysis

SUNTANS is an unstructured grid, three dimensional, nonhydrostatic, constant z-level, parallel model [26]. SUNTANS solves the three-dimensional Reynolds-averaged Navier-Stokes

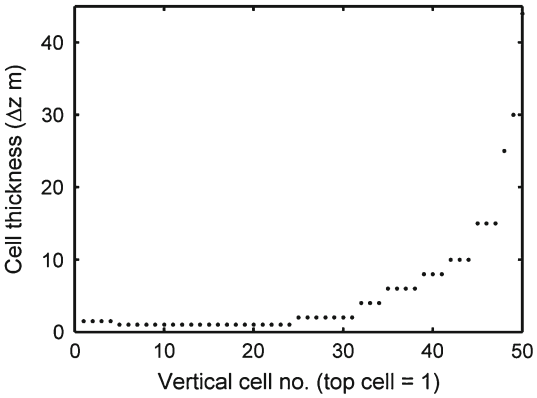

Fig. 9 Vertical discretization of the domain. 50 z-levels were used. Each *dot* represents vertical cell thickness

equations under the Boussinesq approximation. It uses a triangular grid in the horizontal. In the vertical direction, z-levels are used and in between these z-levels, the triangles are extruded to form prismatic elements. All the variables except the face normal velocities are stored at the cell centers. An unstructured grid with a mean horizontal resolution of 1550 m was used. The maximum resolution is 2640 m and the minimum resolution is 307 m. 50 z-levels were used in the model and the vertical resolution used from top to bottom is shown in Fig. 9 ($4 \times 1.5\,\text{m} + 20 \times 1\,\text{m} + 7 \times 2\,\text{m} + 3 \times 4\,\text{m} + 4 \times 6\,\text{m} + 3 \times 8\,\text{m} + 3 \times 10\,\text{m} + 3 \times 15\,\text{m} + 1 \times 25\,\text{m} + 1 \times 30\,\text{m} + 1 \times 44\,\text{m}$). The total three-dimensional grid points were 7,55,630 and a single processor was used for performing the simulations which took nearly 28 h to finish with a time step size of 20 s and 32,400 total time steps. The unresolved sub-grid-scale horizontal turbulent mixing of momentum and heat is modeled with a constant eddy viscosity and eddy diffusivity, respectively. The constant horizontal eddy viscosity used was $10\,\text{m}^2/\,\text{s}$ and the horizontal eddy diffusivity for temperature was set as zero as the first order upwinding scheme was used for advection of temperature. The Mellor–Yamada 2.5 [29] turbulence closure parameterization with stability functions modified by Galperin et al. [30] is used to compute the vertical thermal diffusivity. Bottom drag is specified in the form of bottom roughness, which is converted into friction velocity using the log law. A bottom roughness value of 1mm was used (Troy, in preparation).

Three different vertical temperature stratifications were used as initial conditions in the simulations (Fig. 10); these profiles were chosen from historical data in order to simulate the

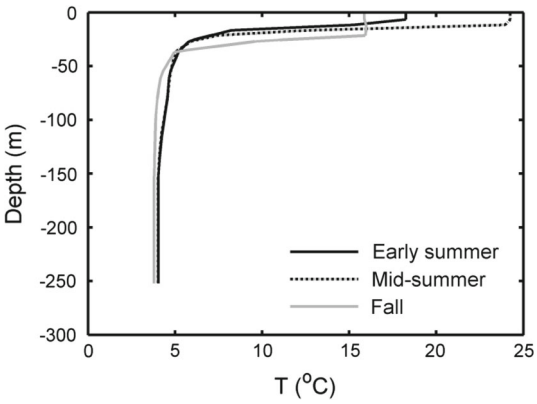

Fig. 10 Temperature initializations used for early summer, mid-summer and fall case studies

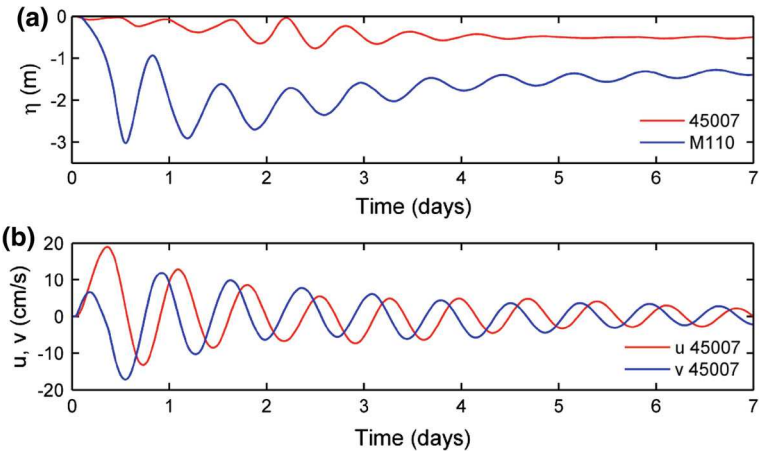

Fig. 11 **a** Raw isothermal displacement of 12.5 °C isotherm at 45007 and M110 locations for the normal bathymetry case. **b** Raw velocities at 10 m depth at 45007 for the normal bathymetry case

periods of early summer (late June), mid-summer (August) and fall (late September). The simulations showed little difference between these three stratifications, so only the mid-summer simulation will be discussed (hereafter "the normal bathymetry case"). The initialized temperature field was assumed to be horizontally uniform throughout the lake, along with a zero magnitude initial velocity field.

Poincaré waves are most effectively generated whenever a sudden wind impulse lasts less than half an inertial period [31], which is approximately 9 h for Lake Michigan. As idealized forcing, a spatially uniform, constant-direction wind burst that ramped up linearly to $0.2\,\mathrm{N/m^2}$ over 0.5 h, remained constant at $0.2\,\mathrm{N/m^2}$ for the next 8 h and then ramped down linearly to zero in the final 0.5 h was used to force the model. The maximum wind stress ($0.2\,\mathrm{N/m^2}$) was chosen to be large enough to generate a strong Poincaré response without causing excessive nearshore velocities (coastal jets) or upwellings. Wind bursts from the east, south, north, and west were considered, with bursts from the south and west being most representative of summer [20]. The duration of the simulations was one week, which is in keeping with the generally observed duration of energetic internal Poincaré wave episodes [17]. Heat exchange with the atmosphere and river inflows were both neglected because of the relatively short (1 week) duration of the simulations.

3.2 Simulated lateral modal structure

Figure 11 shows typical simulated isotherm deflection and velocity response time series for a simulation. For most quantities discussed below, the near-inertial (band-passed) simulation results were interrogated for the 2–3 periods following the cessation of the wind impulse, when the oscillations were no longer forced. Wave phases and amplitudes were determined by simple inspection of wave crests and arrival times (other techniques such as Hilbert Transforms were also tried and they yielded very similar results so the simplest method was adopted).

As shown by Schwab [13] for a flat-bottomed Lake Erie and Gomez-Giraldo et al. [12] for Lake Kinneret/Sea of Galilee, the dominant internal Poincaré waves in lakes with multiple basins tend to be whole-basin modes and separate-basin modes. The numerical simulations

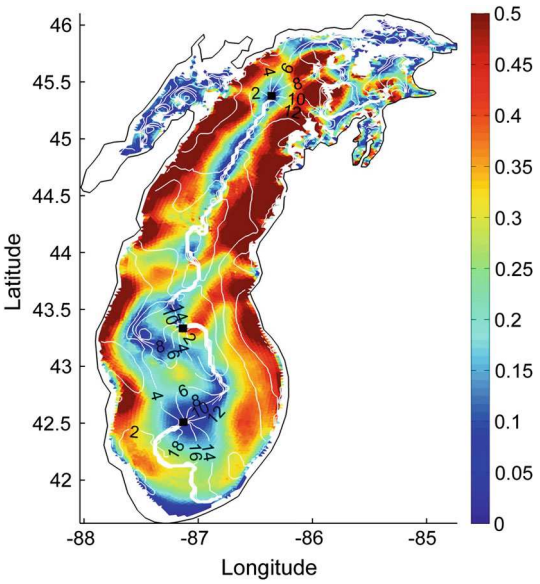

Fig. 12 Near-inertial band pass filtered 12.5 °C isothermal displacement magnitudes (m) and time lines (h) for the normal bathymetry case. The isothermal displacement shown is the maximum value of the amplitude seen during the third inertial period. Time lines (phase; in h) are obtained from the crest arrival time at each location. Three nodes (*square symbols*) are found, with clockwise phase propagation around each node

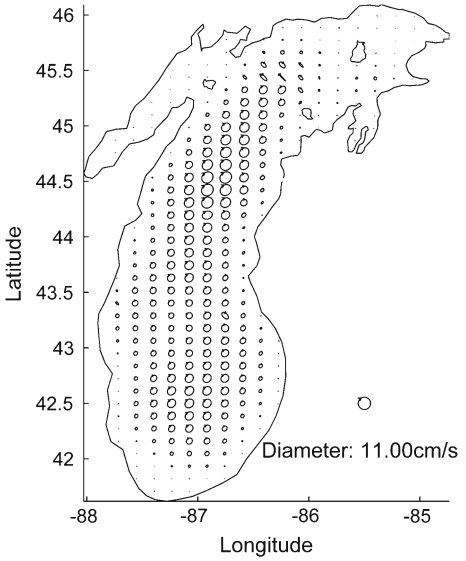

Fig. 13 Current ellipses for the combined near-inertial Poincaré modes in Lake Michigan as perceived at 10 m depth for the same case after three inertial periods. The *arrows* on the ellipses show propagation in clockwise direction

carried out here reveal similar structure for Lake Michigan; however, because of Lake Michigan's size and subsequently low Burger number, both the whole-basin and separate-basin modes have near-inertial frequency and are therefore difficult to separate spectrally for the short-duration simulations.

Figures 12 and 13 show the calculated lateral structure for the dominant near-inertial response of the thermocline displacement and surface currents, respectively. The thermocline displacement map calculation is noisy because of the relatively low isotherm displacements associated with the short-duration wind burst used to generate the waves, but certain features can be identified for the main basin of the lake. The dominant isothermal displacement

structure is seen to be that of transverse mode 1, with high thermocline deflections on the east and west shores, and some bathymetric modification to this basic structure (east-west thermal transects additionally validate this observation). Mode 1 has highest thermocline displacements nearshore, with largest amplitudes on the east and west shores. As discussed below, three primary nodes are seen, as regions of zero thermocline displacement within the lake's interior.

Maps of the simulation-derived wave phase, while noisy, show three amphidromic or nodal points: separate nodes in the centers of the northern and southern basins, and a single central node near the mid-lake plateau (Fig. 12). Following the results by Schwab [13] for Lake Erie, it seems most plausible that the seen response is a superposition of a whole-basin mode and a double-basin mode. The phase progression about all of the nodes appears to be clockwise/anti-cyclonic; this is the expected direction for the lowest-mode internal Poincaré wave cells resulting from an impulsive, spatially-uniform wind stress [10]. The phase progression about the center amphidrome is difficult to discern because of the interaction between the whole-basin mode and the double-basin mode, which have opposing phase propagation directions between the central nodes and the individual basin modes; in general the wave phases near the amphidromes are difficult to discern simply because these regions are nodes in thermocline displacement. Ongoing work seeks to better elucidate this structure using historical simulations, an approach which has the advantage of having larger thermocline displacements due to the accumulation of wind energy over long periods (as in reality), but the disadvantage of having numerous additional physical processes present (e.g. upwellings, coastal jets), which cause additional challenges in their removal.

To clarify the structure associated with the whole-basin mode, simulations were carried out on a flat-bottomed Lake Michigan (hereafter "the uniform depth case"), with the depth taken to be constant at 100 m such that the same vertical grid (the top 40 z-levels) could be used as in the normal bathymetry case. The response for this simulation is much cleaner, basically a single-celled mode with one thermocline displacement node near the mid-lake plateau, approximately at 43° latitude (Fig. 14). Currents are seen to be largest along the major axis of the lake, with little variation along the nodal axis of the seiche, and with maximum thermocline displacements along the east and west lake shores. This simulation shows clockwise phase propagation that is manifested primarily as east-west (i.e. standing) phase propagation because of the lake's high aspect ratio. The structure found in these flat bottomed simulations—namely the absence of basin Poincaré cells—confirms, perhaps not surprisingly, that it is the presence of the lake's double-basin bathymetry that leads to the formation of the basin Poincaré cells, and that spatially variable wind-forcing would be required to create such a structure in such a lake with a single basin.

3.3 Wave-induced velocities

Current ellipses for the combined modes (whole-lake + double-basin) are shown for 10 m depth in Fig. 13, for the normal bathymetry case. In the southern basin and the northern basin, near-inertial circles are seen. The largest velocities occur in the center of the northern basin, followed by the southern basin. This result mirrors the bathymetry of the lake.

Surface velocities were band-pass filtered in the near-inertial region and the kinetic energy was calculated. The RMS (over an inertial period) of these kinetic energies was taken to obtain a map of the surface kinetic energy distribution, which is shown in Fig. 15 (panel a). Irrespective of the season (stratification), the same spatial structure was seen in the maps, indicating that while seasonal changes in stratification change the magnitude of near-inertial motion [10,17], but not the spatial modal structure. The maps generated indicate a large

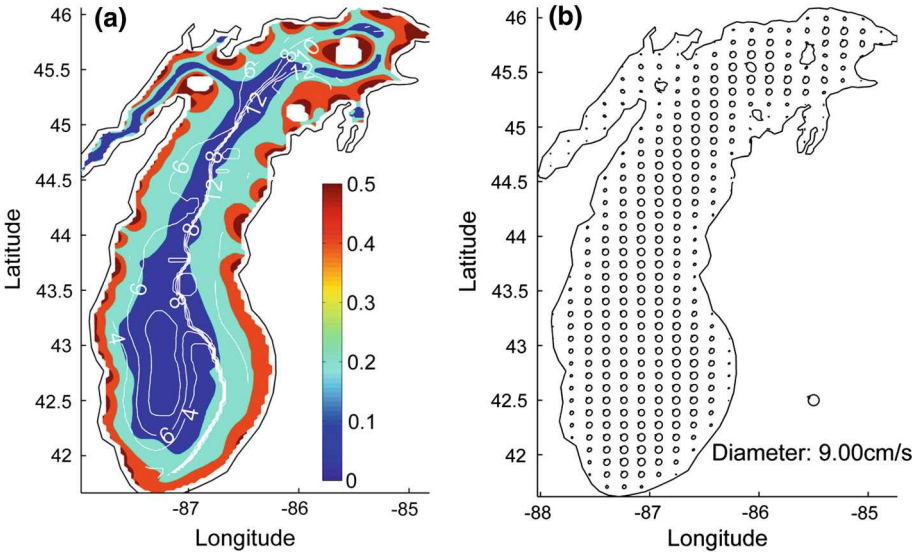

Fig. 14 **a** Isothermal displacement and time lines (h) for the uniform depth case. Isothermal displacement shown is the maximum value of the amplitude seen during the third inertial period. Time lines are obtained from the crest arrival time at each location. *Color bar* shows isothermal displacement in meters. **b** Current ellipses for the near-inertial internal Poincaré mode in Lake Michigan as perceived at 10 m depth for the uniform depth case after three inertial periods. The *arrows* on the ellipses show propagation in clockwise direction

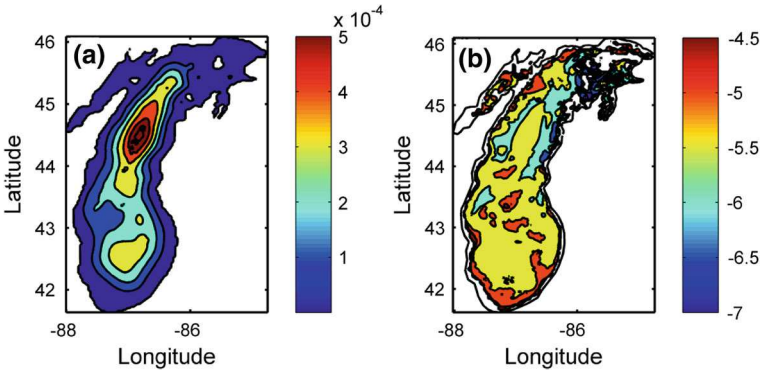

Fig. 15 **a** Surface near-inertial RMS kinetic energy after the third inertial period for the normal bathymetry case. The units of color bar are m^2/s^2. **b** Near-bottom near-inertial $\log_{10}$ (RMS kinetic energy) after the third inertial period for the normal bathymetry case. The units of *color bar* are $\log_{10}(m^2/s^2)$. Log_{10} scale was used to show the variation of near-bottom energy with bathymetry

concentration of energy in the northern and southern basins with very little energy in the shallows in the near-inertial band, as is the case for flat-bottomed basins [9].

The near-bottom velocities induced by the wave are important for determining the persistent spatial influence of the wave on sediment resuspension and benthic exchange of nutrients, pollutants, and biota. Because SUNTANS is a z-level model, and because z-levels in the deep portions of the lake are large and near-bottom flows there are not well resolved,

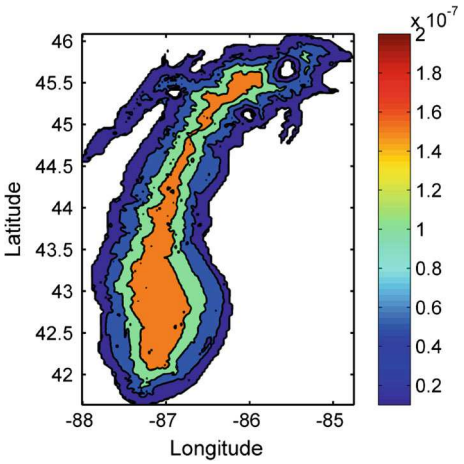

Fig. 16 RMS of squared shear after the third inertial period for the normal bathymetry case. The units of *color bar* are s^{-2}

a normal-modes solution-based approach was used to infer near-bottom velocities from surface velocities (which are well-resolved by the model). Following Choi et al. [17] and other subsequent work by the authors, the normal modes solutions have been shown to provide a reasonable approximation to the vertical structure associated with internal Poincaré waves in Lake Michigan. Using this approach, the normal modes solution was used to calculate the depth-dependent surface-to-bottom velocity ratio, and this ratio was then applied to the surface currents calculated by the model in order to infer near-bottom velocity magnitudes.

The near-bottom energy distribution (Fig. 15, panel b) roughly resembles the lake bathymetry (Fig. 1), i.e. deep locations have lesser energy as compared with the shallower locations. One perfect example of this is the mid-lake plateau, where we see one of the highest near-bottom near-inertial kinetic energy concentrations. This distribution is explained in Sect. 3.4 using a simple theoretical model of the wave-induced bottom velocities across the basin.

Recent work [17,19] suggests that internal Poincaré waves in large lakes may play a large role in basin-scale vertical mixing across the thermocline. Presumably the basin-scale wave structure of thermocline shear will determine the spatial distribution of this mixing, which is set by the combination of local bathymetry and the cross-basin distribution of wave energy. While the simulations were of modest amplitude and sub-critical Richardson numbers were not expected or seen, the spatial distribution of thermocline shear was examined to determine likely locations of mixing in sub-critical cases. The RMS vertical shear magnitude $\left[\overline{\left(\frac{\partial u}{\partial z}\right)^2 + \left(\frac{\partial v}{\partial z}\right)^2}\right]$ was determined at the location of the thermocline (defined as the location of the maximum Brunt-Väisälä frequency). Figure 16 shows the RMS value of squared shear across the thermocline for the normal bathymetry case during the third inertial period from the beginning of the simulation. Maximum shear was seen to be concentrated along the longitudinal axis of the basin away from the basin shoreline (explained below).

3.4 Theoretical distribution

To lowest order, the transverse distribution of near-bottom velocities and thermocline shear are determined by (1) the transverse distribution of wave energy; (2) the stratification; and (3) the transverse depth distribution. To examine these effects, a simple conceptual model

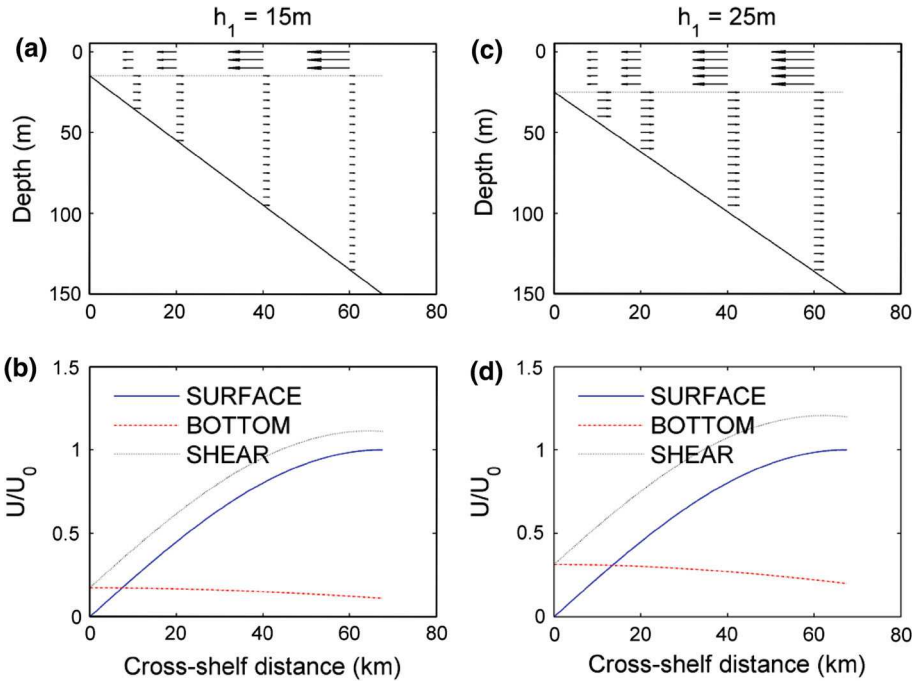

Fig. 17 Theoretical distributions of cross-basin internal Poincaré wave-induced surface velocities (assumed), bottom velocities, and thermocline shear. The simple model predicts maximum thermocline shear in the lake center and relatively constant near-bottom velocities across the basin. Velocities are normalized relative to the maximum (mid-lake) surface velocity

was developed for a seiche in a two-layer stratification in an attempt to explain some of the transverse variability observed in the simulations.

As a simple analysis of the competing effects of transverse wave variability and bathymetry, we consider a simple two-layer stratification with epilimnion thickness h and cross-shelf total depth profile $H(y)$. Following Mortimer [15] and Gill [32], we make a simple assumption that the lowest transverse Poincaré-wave mode near-surface velocity varies across the basin as:

$$U_{surf} = U_0 \sin\left(\frac{\pi y}{W}\right) \tag{4}$$

where y is taken as the distance from the thermocline-shelf intersection location, U_0 is the magnitude of the mid-lake wave-induced surface velocity (at $y = \frac{W}{2}$), and W is the lake width (Fig. 17). To lowest order, the vertically-integrated net flow for the baroclinic wave field must be zero, and therefore the magnitudes of the local baroclinic surface (U_{surf}) and bottom (U_{bot}) velocities are related in the usual manner as

$$U_{bot}\,(H - h) = U_{surf}\,h \tag{5}$$

This implies that the hypolimnetic baroclinic velocity should vary across the lake shelf as

$$U_{bot} = U_0 \sin\left(\frac{\pi y}{W}\right)\left(\frac{h}{H\,(y) - h}\right). \tag{6}$$

In particular, if the water depth varies linearly as $H = h + \alpha y$, where α is the bathymetric slope, the bottom baroclinic velocity will vary as

$$U_{bot} = U_0 \sin\left(\frac{\pi y}{W}\right)\left(\frac{h}{\alpha y}\right) \tag{7}$$

There are several results from this simple model, which is shown in Fig. 17 for two mixed layer thicknesses ($h_1 = 15.25$ m) for a linear bathymetric profile roughly similar to that of Lake Michigan's southern basin. Firstly, near-bottom near-inertial energy is predicted to be a maximum at the thermocline-shelf intersection, and to decay only very weakly with cross-shelf distance from this location. Thus, the conceptual model does not predict strong cross-shelf gradients in near-bottom energy, which is similar to the distribution given by the numerical model (Fig. 17). Additionally, the conceptual model yields maximum thermocline shear (effectively the sum of the magnitudes of the bottom and surface velocities) at the lake interior, which also agrees well with the simulations (Fig. 17).

For deeper mixed layers as are found in fall, two effects occur: (1) the near-bottom near-inertial maximum moves offshore with the thermocline-shelf intersection; and (2) near-bottom velocities are everywhere larger relative to the maximum mid-lake mixed layer velocities. The above arguments are most useful in predicting the cross-shelf variation in near-inertial energy at various times during the year. The actual seasonal distribution of near-inertial near-bottom energies at a given location will therefore be set by the above (spatial) effects and the seasonal variability of both the thermocline-shelf intersection as well as the level of near-inertial energy in the lake (which sets the maximum mid-lake velocity U_0 by which the solution (7) is scaled). The combination of the above factors suggests that near-inertial waves will induce the largest near-bottom velocities at deeper depths in fall, when near-inertial energy in the lake is still large, and the thermocline has moved offshore a significant distance.

The cross-shelf variation in near-bottom near-inertial energy that is actually observed will be complicated further by complex bathymetry, which alters not only the epilimnetic/hypolimnetic velocity ratio (5), but also sets the basin-scale structure of the wave (assumed here as (4)).

4 Summary and conclusions

Field observations and numerical simulations were used in order to determine the vertical and lateral structure of the near-inertial internal Poincaré wave response in Lake Michigan. Data was collected from shallow (<110 m) locations in the southern basin of Lake Michigan at Michigan City (IN) during 2009 and Muskegon (MI) during 2010. Super-inertial isotherm displacements at these locations were found to be almost entirely dominated by near-inertial waves. The isothermal displacements at all the thermistor chain locations were found to be of modest amplitude, on average 2 m or less, and roughly constant across the lake shelf. These results are in keeping with analytical results from flat-bottomed, stratified basins [9], suggesting that actual sloping lake bottoms do not substantially change those results. Analysis of velocities measured in relatively shallow waters (30 m depth) shows that the strong influence of the near-inertial seiche persists almost to the thermocline-shelf intersection.

EOF analysis of the velocity data during the 2009 field experiment indicated the dominance of baroclinic vertical mode 1 over all other modes, with the vast majority of the observed super-inertial kinetic energy attributed to that mode. This vertical mode 1 structure rotates clockwise at near-inertial period, inducing substantial shear in the thermocline. Nearly 90 % of

the super-inertial variance was explained by the first vertical baroclinic mode during periods of intense near-inertial activity. No evidence was found to indicate the presence vertical mode 2 waves. Additionally, complex EOF analysis revealed a persistent phase-locked velocity spiral within the thermocline and hypolimnion, suggestive of enhanced friction (turbulence) associated with the waves that is manifested in the form of a rotating Ekman spiral. As a related finding, it was found that this thermocline spiral will be manifested as spurious mode 2 energy if EOF analysis is not carried out simultaneously on the complex velocity fields and is instead carried out on individual east or north velocity fields.

Numerical simulations were performed using the 3D hydrodynamic code SUNTANS to identify the dominant lateral structure of internal Poincaré wave modes excited by idealized forcing. For the impulsive forcing used, the broad spatial structure of the response was found to be insensitive to both the wind direction and thermal stratification. The basic response, while somewhat noisy because of the relatively low-energy simulations, appeared as a combination of two near-inertial modes: a whole-basin mode and a co-rotating two-basin mode, similar to that found for Lake Erie by Schwab [13]. The combined structure has largest surface kinetic energy in the center of the northern and southern lake basins, and largest, but modest thermocline displacements along the east and west lake shores. Thermocline shear associated with the combined response is also concentrated at these locations, suggesting that the near-inertial wave impact on cross-thermocline mixing may be largest at mid-basin.

A simple conceptual model of the cross-lake distribution of near-bottom internal Poincaré wave energy suggests approximately constant wave-induced near-bottom velocities across the basin, and maximum thermocline shear mid-basin. This finding suggests that the middle of Lake Michigan may be a location of greatly elevated mixing from internal Poincare waves, as suggested by Choi et al. [17], and additional measurements are needed to corroborate this hypothesis. This conceptual model agrees reasonably well with the simulated transverse variability of near-bottom velocities, suggesting that the near-bottom influence of the waves is relatively constant across the basin. Historical (non-idealized) simulations are needed to further examine the effects of actual wind fields and their spatio-temporal distribution on the excitation of these basin scale modes.

Acknowledgments The authors wish to thank the crew of the National Oceanographic and Atmospheric Administration (NOAA) Great Lakes Environmental Research Lab (GLERL) R/V Laurentian for their help with mooring deployment and recovery. This work was supported by the Physical Oceanography Division of the National Science Foundation, grant OCE-1030842. This work is NOAA-GLERL contribution #1668.

References

1. Heaps NS, Ramsbottom AE (1966) Wind effects on water in a narrow two-layered lake. Phil Trans R Soc Lond Ser A 259:391–430
2. Imberger J (1998) Flux paths in a stratified lake. Coast Estuar Stud 54:1–17
3. Shimizu K, Imberger J (2008) Energetics and damping of basin-scale internal waves in a strongly stratified lake. Limnol Oceanogr 53(4):1574–1588
4. Gloor M, Wüest A, Munnich M (1994) Benthic boundary mixing and resuspension induced by internal seiches. Hydrobiology 284:59–68
5. Hawley N (2004) Response of the benthic nepheloid layer to near-inertial internal waves in southern Lake Michigan. J Geophys Res 109:C04007
6. Lorke A, Muller B, Maerki M, Wuest A (2003) Breathing sediments: the control of diffusive transport across the sediment-water interface by periodic boundary-layer turbulence. Limnol Oceanogr 48: 2077–2085
7. Gloor M, Wuest A, Imboden DM (2000) Dynamics of mixed bottom boundary layers and its implications for diapycnal transport in a stratified, natural water basin. J Geophys Res 105:8629–8646

8. Lemckert C, Antenucci J, Saggio A, Imberger J (2004) Physical properties of turbulent benthic boundary layers generated by internal waves. J Hydraul Eng 130:58–69
9. Antenucci JP, Imberger J (2001) Energetics of long internal gravity waves in large lakes. Limnol Oceanogr 46(7):1760–1773
10. Csanady G (1972) Response of large stratified Lakes to Wind. J Phys Oceanogr 2:3–13
11. Fricker PD, Nepf HM (2000) Bathymetry, stratification, and internal seiche structure. J Geophys Res 105(C6):14237–14251
12. Gomez-Giraldo A, Imberger J, Antenucci J (2006) Spatial structure of the dominant basin-scale internal waves in Lake Kinneret. Limnol Oceanogr 51(1):229–246
13. Schwab DJ (1977) Internal free oscillations in Lake Ontario. Limnol Oceanogr 22(4):700–708
14. Boyce FM, Chiocchio F (1987) Inertial frequency current oscillations in the central basin of Lake Erie. J Great Lakes Res 13(4):542–558
15. Mortimer CH (2004) Lake Michigan in motion-responses of an inland sea to weather, earth-spin, and human activities. The University of Wisconsin Press, Madison
16. Mortimer CH (2006) Inertial oscillations and related internal beat pulsations and surges in Lakes Michigan and Ontario. Limnol Oceanogr 51:1941–1955
17. Choi J, Troy CD, Hsieh T-C, Hawley N, McCormick MJ (2012) A year of internal Poincaré waves in southern Lake Michigan. J Geophys Res 117: C07014. doi:10.1029/2012JC007984
18. Austin J (2013) Observations of near-inertial energy in Lake Superior. Limnol Ocean 58(2):715–728
19. Bouffard D, Boegman L, Rao YR (2012) Poincaré wave induced mixing in a large lake. Limnol Oceanogr 57(4):1201–1216
20. Troy CD, Ahmed S, Hawley N, Goodwell A (2012) Cross-shelf thermal structure in Lake Michigan during the stratified periods. J Geophys Res 117:C02028
21. Wüest A, Lorke A (2003) Small-scale hydrodynamics in lakes. Annu Rev Fluid Mech 35:373–412. doi:10.1146/annurev.fluid.35.101101.161220
22. Beletsky D, Schwab DJ (2001) Modeling circulation and thermal structure in Lake Michigan: annual cycle and interannual variability. J Geophys Res 106(C9):19745–19771
23. Edwards CR, Seim HE (2008) Complex EOF analysis as a method to separate barotropic and baroclinic velocity structure in shallow water. J Atmos Ocean Tech 25:805–821
24. Kundu PK, Allen JS (1976) Some three-dimensional characteristics of low frequency current fluctuations near the Oregon coast. J Phys Oceanogr 6:181–199
25. Antenucci JP, Imberger J, Saggio A (2000) Seasonal evolution of the basin-scale internal wave field in a large stratified lake. Limnol Oceanogr 45(7):1621–1638
26. Fringer OB, Gerritsen M, Street RL (2006) An unstructured-grid, finite-volume, nonhydrostatic, parallel coastal ocean simulator. Ocean Model 14(3–4):139–278
27. Ahmed S (2013) Investigations of seasonal and episodic variability in Lake Michigan currents and temperatures. PhD dissertation. Purdue University, p 273
28. Beletsky D, O'Connor WP, Schwab DJ, Dietrich DE (1997) Numerical simulation of internal Kelvin waves and coastal upwelling fronts. J Phys Oceanogr 27:1197–1215
29. Mellor GL, Yamada T (1982) Development of a turbulence closure model for geophysical fluid problems. Rev Geophys Space Phys 20(4):851–875
30. Galperin B, Kantha LH, Hassid S, Rosati A (1988) A quasi-equilibrium turbulent energy model for geophysical flows. J Atmos Sci 45:55–62
31. Boyce FM, Donelan MA, Hamblin PF, Murthy CR, Simons TJ (1989) Thermal structure and circulation in the Great Lakes. Atmos Ocean 27(4):607–642
32. Gill AE (1982) Atmosphere-ocean dynamics. International geophysics series. Academic Press, San Diego